

Nature of 4FGL J1838.2+3223: a flaring ‘spider’ pulsar candidate

D. A. Zyuzin^{1*}, A. Yu. Kirichenko^{2,1}, A. V. Karpova¹, Yu. A. Shibano¹, S. V. Zharikov², M. R. Gilfanov^{3,4}, C. Perez Tórtola⁵

¹*Ioffe Institute, Politekhnicheskaya 26, St. Petersburg 194021, Russia*

²*Instituto de Astronomía, Universidad Nacional Autónoma de México, Apdo. Postal 877, Ensenada, Baja California, México, 22800*

³*Space Research Institute, Russian Academy of Sciences, Profsoyuznaya 84/32, Moscow 117997, Russia*

⁴*Max-Planck-Institut für Astrophysik, Karl-Schwarzschild-Str. 1, D-85741 Garching, Germany*

⁵*Instituto de Investigación en Ciencias Físicas y Matemáticas, USAC, Ciudad Universitaria, 01012, Zona 12, Guatemala*

Accepted XXX. Received YYY; in original form ZZZ

ABSTRACT

An unidentified γ -ray source 4FGL J1838.2+3223 has been proposed as a pulsar candidate. We present optical time-series multi-band photometry of its likely optical companion obtained with the 2.1-m telescope of Observatorio Astronómico Nacional San Pedro Mártir, Mexico. The observations and the data from the Zwicky Transient Facility revealed the source brightness variability with a period of ≈ 4.02 h likely associated with the orbital motion of the binary system. The folded light curves have a single sine-like peak per period with an amplitude of about three magnitude accompanied by fast sporadic flares up to one magnitude level. We reproduce them modelling the companion heating by the pulsar. As a result, the companion side facing the pulsar is strongly heated up to 11300 ± 400 K, while the temperature of its back side is only 2300 ± 700 K. It has a mass of $0.10 \pm 0.05 M_{\odot}$ and underfills its Roche lobe with a filling factor of $0.60^{+0.10}_{-0.06}$. This implies that 4FGL J1838.2+3223 likely belongs to the ‘spider’ pulsar family. The estimated distance of ≈ 3.1 kpc is compatible with *Gaia* results. We detect a flare from the source in X-rays and ultraviolet using *Swift* archival data and another one in X-rays with the *eROSITA* all-sky survey. Both flares have X-ray luminosity of $\sim 10^{34}$ erg s⁻¹ which is two orders of magnitude higher than the upper limit in quiescence obtained from *eROSITA* assuming spectral shape typical for spider pulsars. If the spider interpretation is correct, these flares are among the strongest flares observed from non-accreting spider pulsars.

Key words: binaries: close – stars: individual: 4FGL J1838.2+3223 – stars: neutron – X-rays: binaries

1 INTRODUCTION

To date, the *Fermi* Gamma-ray Space Telescope has detected 144 millisecond pulsars (MSPs) (Smith et al. 2023). Among them, the subclass of so-called ‘spider’ pulsars is of particular interest (Roberts 2013). It includes black widows (BWs) and redbacks (RBs) which are compact binaries with orbital periods $P_b < 1$ d where one side of the companion star is heated by the pulsar wind. BWs have very low-mass ($M_c \lesssim 0.05 M_{\odot}$) semi-degenerate companions while RBs have non-degenerate and more massive ($M_c \approx 0.1$ – $1 M_{\odot}$) companions. Some RBs show transitions between radio-pulsar and accreting modes (e.g. Archibald et al. 2009; Papitto et al. 2013; Bassa et al. 2014; Roy et al. 2015) confirming the low-mass X-ray binaries as progenitors of spider systems. However, details of formation and the evolutionary link between RBs and BWs are not clear and actively discussed (Chen et al. 2013; Benvenuto et al. 2014; Ablimit 2019; Guo et al. 2022). Studies of spider pulsars are also important for constraining the equation of state of the superdense matter inside neutron stars (NSs) since the most massive of them have been found in binary systems (e.g. Romani et al. 2022).

Detection of pulsations from RBs and BWs is a somewhat chal-

lenging task since the pulsar emission is often eclipsed by material ablated from the companion star by the pulsar wind. However, even in the case of non-detection of pulsations, it is possible to identify such systems using optical and X-ray observations of unassociated γ -ray sources (e.g. Salvetti et al. 2017). In particular, optical studies allow one to clarify the spectral type of the companion star, its mass and irradiation efficiency by the pulsar, the distance to the system, the binary inclination, and the pulsar mass. Only about four dozen confirmed spiders and about one dozen of candidates had been detected in the optical so far (Strader et al. 2019; Miller et al. 2020; Swihart et al. 2020, 2021, 2022; Au et al. 2023; Karpova et al. 2023; Yap et al. 2023). Parameters of many of them are poorly constrained due to the faintness of the objects. Thus, new identifications and studies of brighter companions are necessary for investigations of such systems.

Recently, Kerby et al. (2021) built a neural network classifier trained on samples of known pulsars and blazars and used it to classify the unidentified *Fermi* sources. Based on possible X-ray and optical counterparts found with the *Swift* X-ray Telescope (XRT) and UltraViolet Optical Telescope (UVOT), they identified 14 *Fermi* sources for which the probability of being a blazar was less than 1 per cent, thus making them likely pulsar candidates. 4FGL J1838.2+3223 (hereafter J1838) is one of these sources. According to the 4FGL-

* E-mail: da.zyuzin@gmail.com (DAZ)

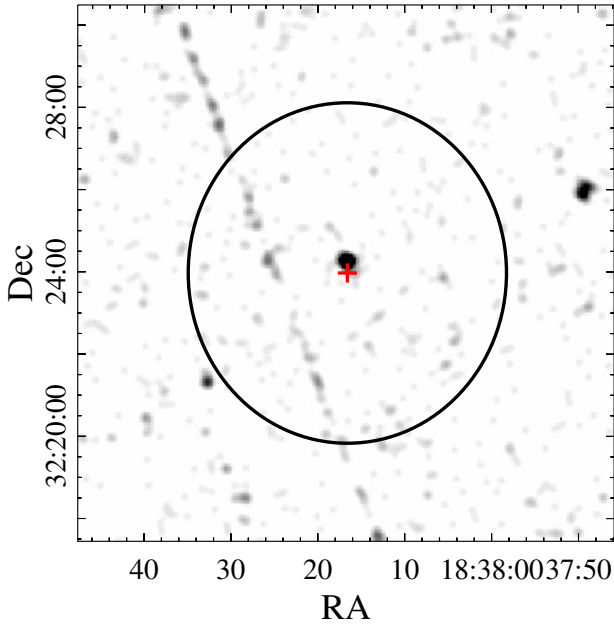


Figure 1. 13×13 arcmin² *Swift*/XRT image of J1838 combined from different observations with the total exposure of 7.6 ks. The red cross and black ellipse show the γ -ray position of J1838 and its 95 per cent uncertainty. The X-ray counterpart candidate proposed by Kerby et al. (2021) is the nearest point object to the red cross. The stripe crossing the field is an instrumental artifact.

DR3 catalogue, its γ -ray flux in the 0.1–100 GeV range is $F_\gamma = (2.7 \pm 0.6) \times 10^{-12}$ erg s⁻¹ cm⁻² (Abdollahi et al. 2022). The visual brightness of its optical counterpart proposed by Kerby et al. (2021) is 21.3 mag. At the time of the *Swift* observation, the possible X-ray counterpart was the brightest X-ray source in the *Swift*/XRT field of view (23.6×23.6 arcmin²) with the 0.3–10 keV unabsorbed X-ray flux of $F_X \approx 7 \times 10^{-13}$ erg s⁻¹ cm⁻² (Kerby et al. 2021). The proposed counterpart of J1838 is located in ≈ 20 arcsec from the *Fermi* position of J1838, and it is the only X-ray source detected by *Swift* within the 95 per cent error ellipse of the γ -ray pulsar candidate J1838 (Fig. 1).

To clarify the nature of the presumed X-ray and optical counterpart of J1838, we performed multi-band optical observations and multi-epoch analysis of archival X-ray and optical data. The data from catalogues are presented in Sec. 2. Optical observations and data reduction are described in Sec. 3 and the light curves modelling – in Sec. 4. The description of the X-ray and ultraviolet (UV) data is presented in Sec. 5. We discuss and summarise the results in Sec. 6.

2 DATA FROM CATALOGUES

The likely X-ray counterpart of J1838 suggested by Kerby et al. (2021) is nominated in their work as SwXF4 J183817.0+322416. Using the *Swift*/XRT data products generator¹ (Evans et al. 2009) we obtained its coordinates (see Table 1) and the 90 per cent position uncertainty of 4.4 arcsec. Within the uncertainty circle we found the presumed J1838 optical counterpart in the Panoramic Survey Telescope and Rapid Response System (Pan-STARRS, Flewelling

Table 1. Parameters of the J1838 and its counterpart candidate.

Parameters from the literature	
R.A. in the optical α_{opt}	18 ^h 38 ^m 16 ^s .81807(12)
Dec. in the optical δ_{opt}	+32°24′11″.4148(11)
Galactic longitude l , deg	61.283
Galactic latitude b , deg	16.706
P.m. in R.A. direction $\mu_\alpha \cos \delta$, mas yr ⁻¹	-4.9(2.0)
P.m. in Dec. direction μ_δ , mas yr ⁻¹	-9.9(1.2)
Distance D_{geom} , kpc	1.0–3.5
γ -ray flux F_γ , erg s ⁻¹ cm ⁻²	$2.7(6) \times 10^{-12}$
Parameters derived in this paper	
R.A. in X-rays α_X	18 ^h 38 ^m 16 ^s .71
Dec. in X-rays δ_X	+32°24′1″.8
Orbital period P_b , h	4.02488(15)
X-ray flux (flare) F_X^{flare} , erg s ⁻¹ cm ⁻²	$\sim 10^{-11}$
X-ray flux (quiescence) F_X , erg s ⁻¹ cm ⁻²	$< 9 \times 10^{-14}$
X-ray luminosity (flare) L_X^{flare} , ($D/3.1$ kpc) ² erg s ⁻¹	$\sim 10^{34}$
X-ray luminosity (quiescence) L_X , ($D/3.1$ kpc) ² erg s ⁻¹	$< 10^{32}$
γ -ray luminosity L_γ , ($D/3.1$ kpc) ² erg s ⁻¹	$3.1(7) \times 10^{33}$

Hereafter numbers in parentheses denote 1σ uncertainties relating to the last significant digit.

The optical coordinates and the proper motion (p.m.) are obtained from the *Gaia* catalogue.

F_X and F_X^{flare} are the unabsorbed fluxes in the 0.5–10 keV range and F_γ is the flux in the 0.1–100 GeV range.

et al. 2020) with ID 146882795700574433, which can also be cross-identified in *Gaia* (Gaia Collaboration et al. 2016, 2021) and Zwicky Transient Facility (ZTF, Masci et al. 2019) archive data. Its parameters are presented in Table 1. In the Pan-STARRS catalogue its mean AB magnitudes are $g = 20.7(1)$, $r = 20.46(6)$, $i = 20.43(5)$ and $z = 20.5(1)$. These are apparently brighter than $m_V = 21.3$ reported by Kerby et al. (2021). However, based on individual Pan-STARRS detections the source shows variability at a level of 1–2 stellar magnitude. The ZTF data confirm the variability.

The ‘geometric’ distance D_{geom} obtained with *Gaia* lies in the range 1–3.5 kpc, while the ‘photogeometric’ distance D_{pgeom} is 8.7–12.4 kpc. The proper motion $\mu = 11.1 \pm 1.4$ mas yr⁻¹ transforms to the transverse velocity of about 50–200 km s⁻¹ for D_{geom} and 500–700 km s⁻¹ for D_{pgeom} . The latter is much larger than expected from the velocity distribution for binary systems with pulsars (Hobbs et al. 2005). This suggests that the photogeometric distance is unrealistic and we excluded it from consideration. For D_{geom} , the J1838 γ -ray luminosity is $L_\gamma = (0.3\text{--}4) \times 10^{33}$ erg s⁻¹ and the X-ray luminosity obtained from the flux derived by Kerby et al. (2021) is $L_X \approx 10^{32}\text{--}10^{33}$ erg s⁻¹. Such parameters are typical for the spider pulsar family (Strader et al. 2019; Swihart et al. 2022).

3 OPTICAL OBSERVATIONS AND DATA REDUCTION

The time-series photometric observations of J1838 were performed using the *BVRI* Johnson-Cousins bands with the ‘Rueda Italiana’

¹ https://www.swift.ac.uk/user_objects/

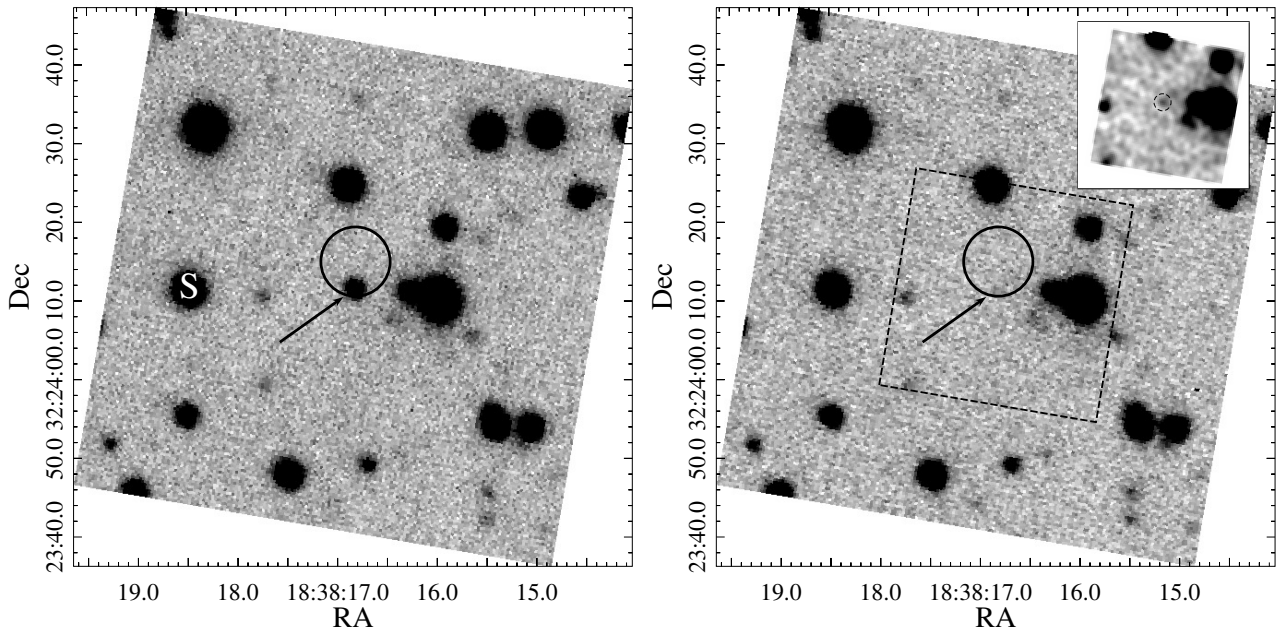


Figure 2. Individual R -band images of the J1838 field obtained with the OAN-SPM telescope during the maximum (left) and the minimum (right) brightness phases of the likely optical counterpart marked by the arrow. The solid circle with a radius of 4.4 arcsec shows the *Swift*/XRT 90 per cent position uncertainty of the J1838 X-ray counterpart candidate; ‘S’ in the left panel denotes the star used as the secondary photometric standard in this work. The region enclosed in the dashed box in the right panel is shown in the inset with a different intensity scale to better reveal the candidate (marked with the dashed circle) at the phase of its minimum brightness.

Table 2. Log of the J1838 observations with the OAN-SPM 2.1-m telescope.

Date YYYY/MM/DD	Filter	Number of exposures	Airmass	Seeing, arcsec
2022/07/21	B	3	1.0–1.5	1.2–1.4
	V	18	1.0–1.3	
	R	8	1.0–1.5	
	I	4	1.0–1.4	
2022/07/22	B	5	1.0–1.5	1.5–1.7
	V	6	1.0–1.3	
	R	30	1.0–1.5	
	I	6	1.0–1.3	
2022/07/24	B	5	1.0–1.1	1.3–1.8
	V	5	1.0–1.2	
	R	30	1.0–1.2	
	I	5	1.1–1.2	

instrument² attached to the 2.1-m telescope at the Observatorio Astronómico Nacional San Pedro Mártir (OAN-SPM), Mexico in July 2022. The field of view of the detector is 6×6 arcmin² with an image scale of 0.34 arcsec in the 2×2 CCD pixel binning mode. The log of observations is given in Table 2. Individual exposures varied from 350 to 700 s.

We carried out standard data processing, including bias subtraction and flat-fielding utilising the IRAF package. In addition, fringe correction was performed for all I -band images. Astrometric solution was calculated using a set of 9 stars from the *Gaia* eDR3 Catalogue (Gaia Collaboration et al. 2016, 2021; Lindegren et al. 2021) with positional errors of $\lesssim 0.13$ mas. Formal *rms* uncertainties of the resulting

astrometric fit were $\Delta\alpha \lesssim 0.04$ arcsec and $\Delta\delta \lesssim 0.05$ arcsec. The photometric calibration was performed using the Landolt standards SA 109-949, 954, 956 (Landolt 1992) observed on 2022 July 22. All the data from the other nights were re-calibrated using a field non-variable star (Pan-STARRS ID 146882795769764297, $r = 17.67(4)$ mag) close to the target as a secondary standard. It is marked by ‘S’ in Fig. 2, left. According to Pan-STARRS its brightness variability is $\Delta m \lesssim 0.1$ mag.

4 IMAGES, LIGHT CURVES AND ORBITAL PERIOD

Representative images of the J1838 field obtained with the OAN-SPM telescope in the R band are shown in Fig. 2. They demonstrate that the J1838 likely optical counterpart is a highly variable source. It is firmly detected in most exposures and appears close to the detection limit of ≈ 23.8 in some others. There is another faint object detected inside the X-ray position uncertainty and located about 2.5 arcsec north-west of the counterpart candidate (see the inset in Fig. 2, right). The source is also visible close to the detection limit in the Pan-STARRS images. We did not find any variability associated with this background object in our data.

The OAN-SPM light curves of the candidate in four bands are presented in Fig. 3. A smooth sine-like brightness variation with an amplitude of several magnitudes is accompanied by a short flaring activity on time-scales of ~ 10 min with the brightness increase by about 1 mag. This short-term variability is especially prominent in the data obtained on 2022 July 24. The data suggest a brightness periodicity of around 4 h. To find the period, we performed a Lomb-Scargle periodogram analysis (Lomb 1976; Scargle 1982) applying the period range 1–24 h. Excluding the most obvious flares in the R -band marked by the circles in Fig. 3, we obtained a period of 4.0246 h.

To justify the period independently, we investigated the data from

² <https://www.astrossp.unam.mx/en/users/instruments/ccd-imaging/filter-wheel-italiana>

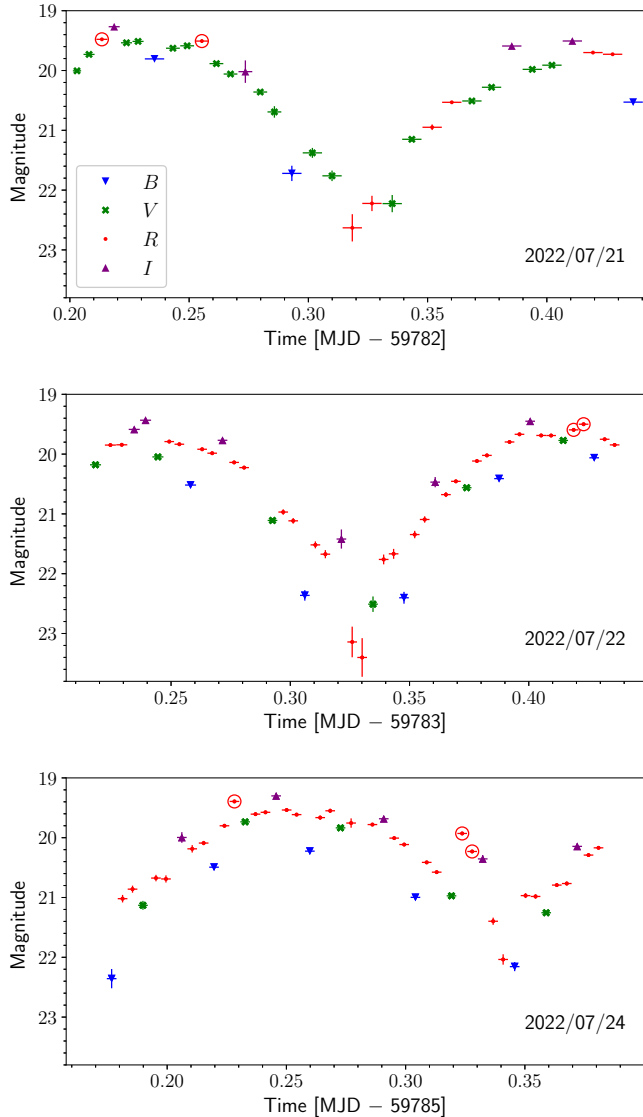


Figure 3. Time-series photometry of the J1838 putative optical counterpart obtained with the OAN-SPM 2.1-m telescope at different dates shown in the panels. Points excluded from the timing analysis are marked with circles (see text).

the ZTF DR16 catalogue which covers about 4.7 yr (MJD 58204–59905) and contains several hundreds of photometric measurements of the source in the *r*-band. The highest peak in the periodogram corresponds to the period $P_{\text{ph}} = 4.02489$ h, which is very close to the value obtained from the OAN-SPM data. However, the power spectrum is noisy, and folding the light curve with the obtained period we found indications of a heavy flaring activity, as has been revealed in the OAN-SPM data. Thus, we excluded ZTF measurements with $r < 19.2$ which are likely related to the flares and recalculated the periodogram. The latter is shown in Fig. 4. The highest peak in the power spectrum at $P_{\text{ph}} = 4.02488$ h is only slightly shifted from the previous estimates and is quite pronounced. Since the *R*-band curve of the OAN-SPM contains only about 60 points, as opposed to the ZTF *r*-band, and covers a much shorter time range, we adopt

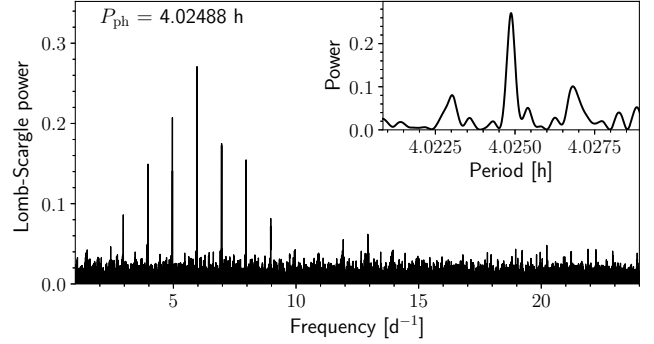


Figure 4. Lomb-Scargle periodogram for the ZTF data in the *r* band calculated excluding points with $r < 19.2$ mag. The best period P_{ph} corresponding to the highest peak, enlarged in the inset, is also indicated.

$P_{\text{ph}} = 4.02488(15)$ h³ obtained from the ZTF data as the true period of the J1838 candidate counterpart.

The ZTF light curves in the *g*, *r* and *i* bands folded with this period are shown in Fig. 5. They demonstrate a single broad peak per period. We calculated the mean binned ZTF light curves and removed all data points with magnitudes 0.3 mag lower than the mean value in each phase bin since they are likely caused by the flaring activity. After that, we calculated the mean binned light curves again - they are compiled together in the bottom panel of Fig. 5. The minima of the ZTF light curves at the orbital phase 0.5 have no detection points. Averaging over larger phase bins artificially smooths and decreases the depth of the minimum (see the bottom panel of Fig. 5).

The light curves obtained with the OAN-SPM are demonstrated in Fig. 6. In this case, deeper observations allowed us to measure the light curves minima more accurately resulting in a total brightness variation of about 3 mag (from ≈ 20 to ≈ 23 mag) in the *R* band.

The period value and shapes of the periodic light curves are typical for a spider pulsar companion owing to its orbital motion around a MSP (e.g. Mata Sánchez et al. 2023; Kandel et al. 2020; Linares et al. 2018). We thus can assume that P_{ph} is an orbital period of J1838. We note, that on 2022 July 24 the source was apparently brighter throughout the whole observation as compared to the two previous nights. This is particularly clearly seen in the *R*-band light curve in Fig. 6 at the phase ranges between about 0.2 and 0.8. It may reflect a global change of the presumed pulsar companion and/or the binary system stage.

4.1 Light-curve modelling

To estimate the parameters of the presumed binary system, we performed the light curve modelling using the technique described in Zharikov et al. (2013, 2019). We modelled only the OAN-SPM data because they are deeper than the ZTF ones and consequently cover the whole period per each observing night. We excluded the data obtained on 2022 July 24 when J1838 was apparently in a different brightness stage.

The model of the system to fit the light curves considers only two components: the NS as the primary and the heated low-mass companion as the secondary. The free parameters were the distance D , the binary system inclination i , the Roche lobe filling factor f , the ‘night-side’ temperature T_{n} of the secondary, the effective irradiation

³ The uncertainty is calculated as the half width at half maximum of the highest peak in the periodogram.

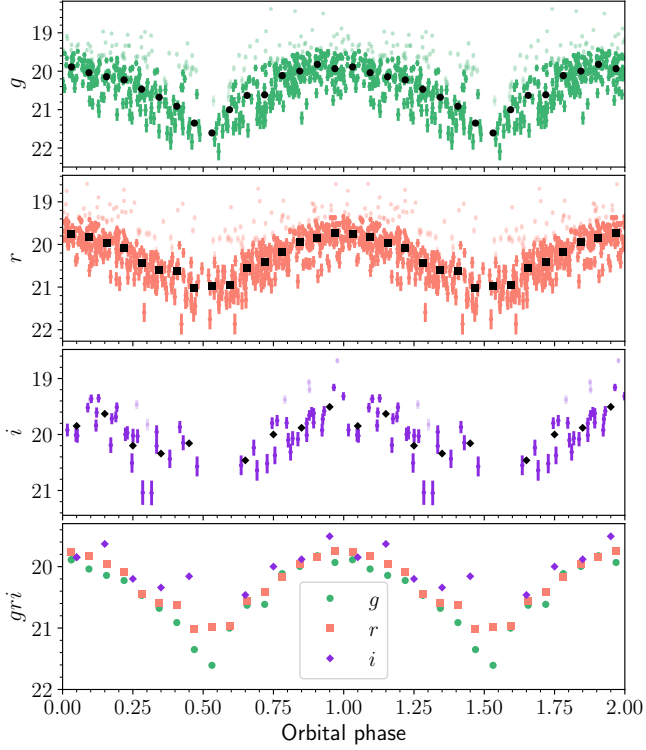


Figure 5. ZTF optical light curves of the J1838 presumed companion in the g , r and i bands (panels 1–3) folded with a period of 4.02488 h. The data points associated with flaring and excluded from analysis are marked by lighter colours. The mean binned light curves are marked by black symbols in panels 1–3 and are shown together in panel 4.

factor K_{irr} [ergs s $^{-1}$ cm $^{-2}$ sr $^{-1}$], the pulsar mass M_{NS} , and mass ratio q . K_{irr} defines the flux F_{in} transferred to the companion:

$$F_{\text{in}} = \cos(\alpha_{\text{norm}})\Omega\Delta SK_{\text{irr}}, \quad (1)$$

where α_{norm} is the angle between the normal to the surface and the incoming flux, $\Omega = \pi R_{\text{NS}}^2/a^2$ is the solid angle from which the NS is visible from the surface element ΔS of the secondary, R_{NS} is the NS radius and a is the orbit separation. The ‘day-side’ temperature of the surface element of the secondary is

$$T_{\text{d}} = T_{\text{n}} \left[1 + \frac{F_{\text{in}}}{\sigma_{\text{SB}}\Delta ST_{\text{n}}^4} \right]^{1/4}, \quad (2)$$

where σ_{SB} is the Stefan-Boltzmann constant. We used the gradient descent method to find the minimum of the χ^2 function:

$$\chi^2 = \sum_j^{B,V,R,I} \sum_k^N \left(\frac{O_k - C_k}{\sigma_k} \right)^2, \quad (3)$$

where O_k , C_k , and σ_k are the observed and the calculated magnitudes, and uncertainties of the observed magnitudes, respectively. We found that the pulsar mass is derived from the fit with a very wide uncertainty of (1–2.7) M_{\odot} making the calculated light curves and the rest of the parameters insensitive to variations of the mass within this range. We thus fixed it at a canonical NS mass of $1.4M_{\odot}$.

The fit results are presented in Table 3 and the left panel of Fig. 7. The parameter uncertainties were calculated following the method proposed by Lampton et al. (1976). As seen from the fit residuals, the calculated light curves are generally consistent with the data, and the minor outliers are likely related to a flaring activity. They are also

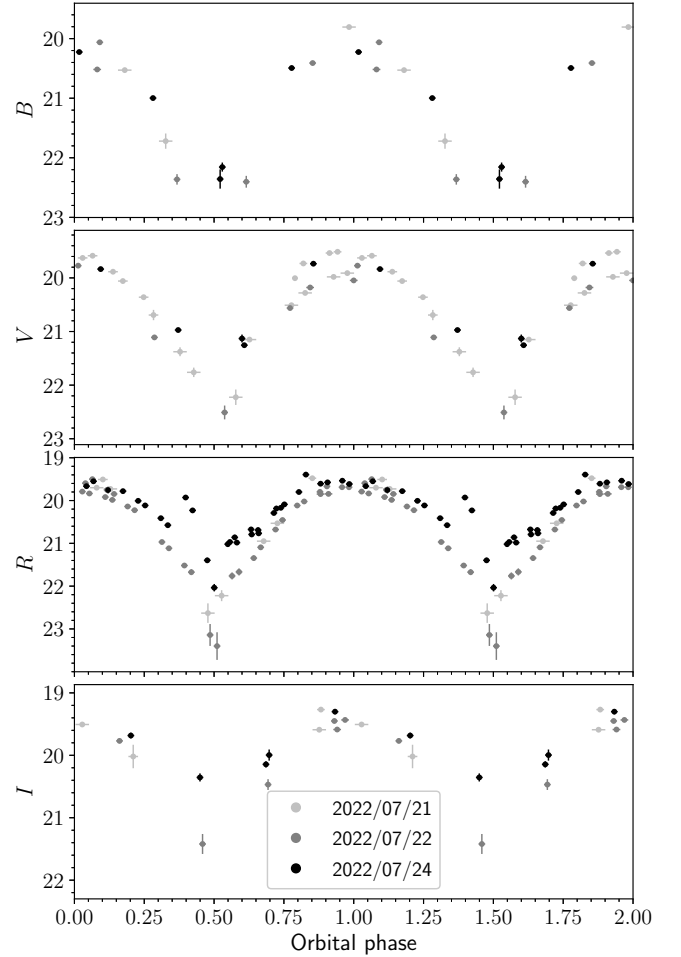


Figure 6. Light curves of the J1838 likely counterpart obtained with the 2.1-meter telescope folded with a period of 4.02488 h. The data obtained during different nights are marked by the different grey colours as indicated in the legend.

compatible with the ZTF data which are noisier and less sensitive as compared to the OAN-SPM data. A noticeable discrepancy is seen only near the minimum brightness phase ($\phi = 0.50 \pm 0.05$) in the R band. The object is reliably ($S/N \approx 4$) detected there (see Fig. 2), but high magnitude uncertainties ($\sigma_k \approx 0.25$ mag) lead to low weights of these points in the fit. This formally results in overshooting the brightness of the model points by about one magnitude in respect to the observed ones.

At the same time, these points can be critically important for convincing constraints of the binary system inclination angle. To study their impact on this parameter, we artificially assigned higher weights to these points, assuming that they could be detected with $\overline{\sigma_k} = 0.09$ mag, which is close to magnitude uncertainties at nearby orbital phases around the minimum, $\phi \in [0.4, 0.45]$ and $\phi \in [0.55, 0.6]$. The result of the respective fit is presented in the right panel of Fig. 7. As seen from the plot, the brightness minimum is better approximated by the model in this case, while the nearby orbital phases are fitted much worse as compared to the initial fit shown in the left panel. It is obvious from this experiment that our light curve model can not account for the brightness dip at the minimum of the light curve. This may be caused by variability of the source light curve or by some effects unaccounted for in the model. Given the variable nature of the J1838 light curve, more photometric data are needed to

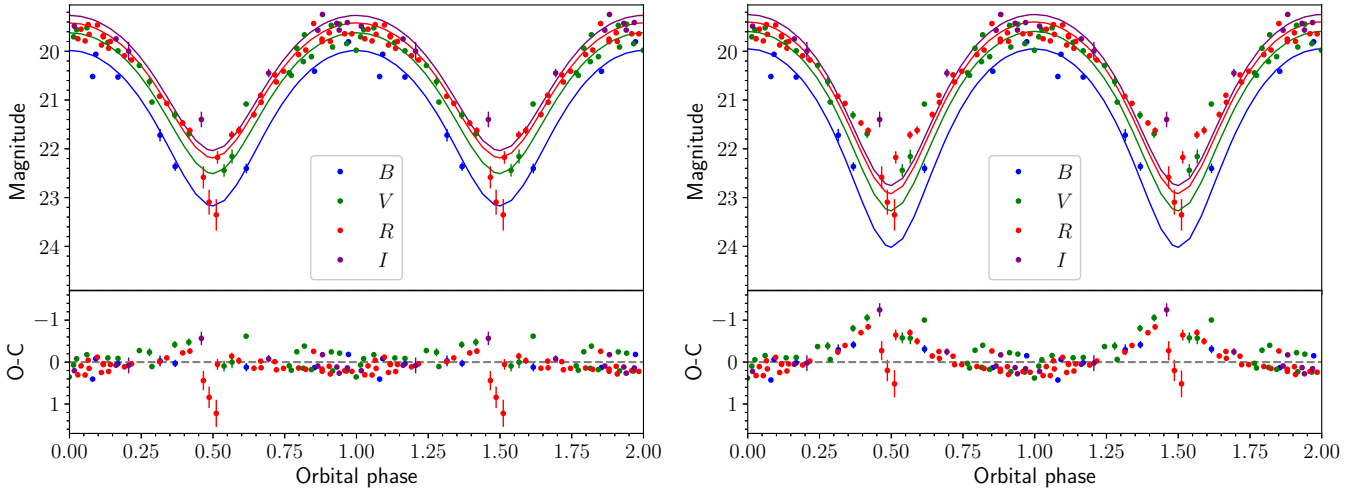


Figure 7. Folded light curves of J1838 obtained in the *B*, *V*, *R* and *I* bands with the OAN-SPM telescope on July 21–22. The solid lines show the best-fitting models. In the right panel, the points at the minimum brightness phase in the *R* band were included in the fit with higher weights (see text). Lower panels show residuals calculated as the difference between the observed (O) and the calculated (C) magnitudes.

Table 3. The light-curve fitting results for J1838.

Fitted parameters	Values
Pulsar mass M_{NS}, M_{\odot} (fixed)	1.4
Mass ratio $q = M_c/M_{\text{NS}}$	0.065(15)
Distance D , kpc	3.1(2)
‘Night-side’ temperature T_n , 10^3 K	2.3(7)
Inclination i , deg	36(10)
Roche lobe filling factor f	$0.60^{+0.10}_{-0.06}$
Irradiation factor K_{irr} , 10^{20} erg cm $^{-2}$ s $^{-1}$ sr $^{-1}$	0.16(3)
Extinction $E(B - V)$, mag	0.092(45)
Derived parameters	
Companion mass M_c, M_{\odot}	0.10(5)
Companion radius R_c, R_{\odot}	0.16(3)
‘Day-side’ temperature:	
Minimum T_d^{min} , 10^3 K	6.0(2)
Maximum T_d^{max} , 10^3 K	11.3(4)

choose between these possibilities. However, within the uncertainties most of the parameters obtained in this test fit remain the same as in the fit without the artificial weights, except for the inclination angle whose best fit value tends to increase by about 10 degrees.

The resulting interstellar colour excess is in agreement with the maximum value in the J1838 direction $E(B - V) = 0.098$ mag following from the dust map of Green et al. (2019). Because of a high stochastic variability of the source, we note that the results of the fit provide only rough constraints on the system parameters. Nevertheless, they are compatible with parameters of other spider systems with modelled light curves.

5 X-RAY AND UV DATA

We re-analysed the X-ray data from *Swift*/XRT and UVOT together with the extended ROentgen Survey with an Imaging Telescope Array

(*eROSITA*; Predehl et al. 2021) aboard Spectrum-Roentgen-Gamma (SRG) orbital observatory (Sunyaev et al. 2021). *Swift*/XRT observed J1838 nine times in 2019 with the total exposure time of ≈ 7.6 ks. SRG/*eROSITA* observed the source field in the course of four all-sky surveys in 2020–2021 with the total exposure time of ≈ 1.3 ks (the vignetting corrected exposure is ≈ 0.7 ks).

Inspection of the *Swift* data revealed that the source is clearly seen only in one data set obtained on 2019 December 12 with the exposure time of 0.85 ks, between the observations on December 8 and 15 (see the top panels of Fig. 8). Thus, the source exhibited a strong flare in X-rays. A similar flaring activity is simultaneously observed in the UV with the UVOT (see the bottom panels of Fig. 8). We measured the AB magnitude during the flare in the *uvw2* band and obtained 20.24(10) mag. Given $E(B - V) = 0.092$ mag (Table 3), the unabsorbed flux is about $70 \mu\text{Jy}$. We note that the position of the UV source perfectly coincides with that of the presumed optical counterpart (Fig. 8) showing that we see the same source in the optical, UV and X-rays.

The X-ray spectrum of the source during the flare was extracted using the *Swift*-XRT data products generator and fitted with the X-Ray Spectral Fitting Package (XSPEC) v.12.11.1 (Arnaud 1996) using an absorbed power-law (PL) model. Only about 30 source counts were obtained in the 0.3–10 keV range. The spectrum was grouped to ensure at least one count per energy bin. For the interstellar absorption, we used the TBABS model with the WILM abundances (Wilms, Allen & McCray 2000). Using the relation from Foight et al. (2016), we transformed $E(B - V)$ from the optical light curve fit to the absorbing column density, $N_{\text{H}} = 8 \times 10^{20}$ cm $^{-2}$, which was fixed during the fitting procedure. The photon index is $\Gamma^{\text{flare}} = 0.5 \pm 0.3$ and the unabsorbed flux in the 0.5–10 keV range is $F_X^{\text{flare}} = 4.5^{+1.5}_{-1.1} \times 10^{-12}$ erg s $^{-1}$ cm $^{-2}$ (errors correspond to the 1σ confidence interval). However, we created the light curve using the online generator and found that the flare took up only about a half of the total exposure (see Fig. 9). Thus, the actual flux of the flare is about two times greater than the one estimated above, $F_X^{\text{flare}} \sim 10^{-11}$ erg s $^{-1}$ cm $^{-2}$.

In the *eROSITA* data J1838 is detected with $\approx 4\sigma$ significance in the 2.3–8 keV band while it is not seen in the soft band (see Fig. 10). Investigating the individual *eROSITA* scans, we found that the source is clearly visible only in the second observation carried out in October

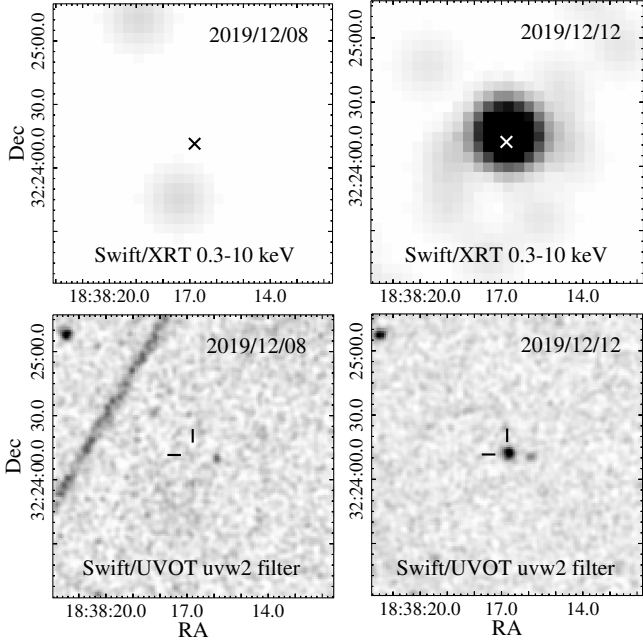


Figure 8. *Swift* XRT (top panels) and UVOT (bottom panels) images of the J1838 field. The position of the J1838 likely optical counterpart is marked by the ‘X’ symbols in the top panels and by the bars in the bottom panels. The bright flare occurred on 2019 December 12. Exposure times are 0.55 ks for the left panels and 0.85 ks for the right panels.

2020 indicating another hard flare (see Fig. 11). We extracted the J1838 spectra from each scan using the *eROSITA* Science Analysis Software System (eSASS). They were binned to ensure at least one count per energy bin. We fitted the spectrum from the second scan with the exposure time of 0.26 ks which contains about 9 counts from the source with the absorbed PL model in the 0.3–10 keV band. N_{H} was fixed at the value mentioned above. We obtained a negative best fit value of the photon index $\Gamma^{\text{flare}} = -1.9^{+0.7}_{-1.0}$ in accord with the fact that the source was detected only in the hard band. The source flux is $F_X^{\text{flare}} = 9^{+9}_{-5} \times 10^{-12} \text{ erg s}^{-1} \text{ cm}^{-2}$. Combining spectra from the other three scans, we derived 90 per cent confidence upper limits on the source flux in quiescence, $F_X \lesssim 9 \times 10^{-14} \text{ erg s}^{-1} \text{ cm}^{-2}$ for $\Gamma = 1.4$ and $F_X \lesssim 3 \times 10^{-14} \text{ erg s}^{-1} \text{ cm}^{-2}$ for $\Gamma = 2.5$. The adopted photon indices are the average values found for BWs and RBs (Swihart et al. 2022).

6 DISCUSSION

Surface density of X-ray sources within the *Swift*/XRT field of view with mean fluxes equal to or higher than the mean flux of the counterpart candidate is 0.0018 per arcmin². Given that, the chance probability to find an unrelated X-ray source within the 95 per cent (4.1×3.9 arcmin²) error ellipse of the γ -ray source is about 8 per cent. Such probability can be even lower if we take into account the strong variability of our source. Medvedev et al. (2022) found only 1325 objects (per a half of sky) from which the flux in the 0.3–2.3 keV energy band changed by more than a factor of 10 during the SRG/*eROSITA* all-sky survey. The reported number transforms to about 1.8×10^{-5} variable objects per arcmin² and the chance probability of 0.1 per cent. This supports the association of the X-ray source and the optical object with the pulsar candidate proposed by Kerby et al. (2021). However, this probability estimation has to be considered with a caution, as the

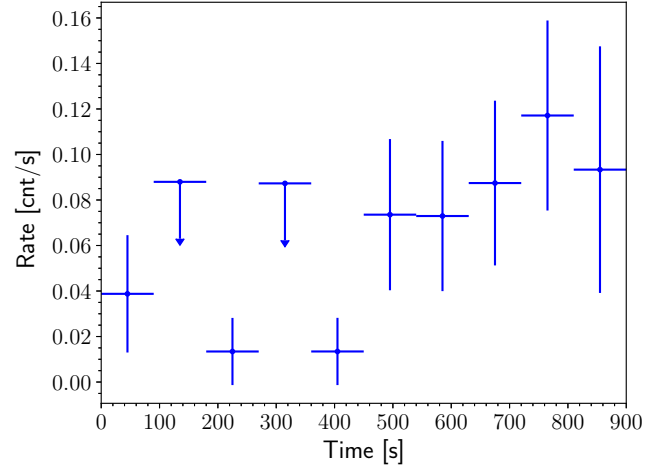


Figure 9. *Swift* XRT light curve of the J1838 putative counterpart during the flare in the 0.3–10 keV band. The time bin size is 90 s. Upper limits correspond to 3σ confidence levels.

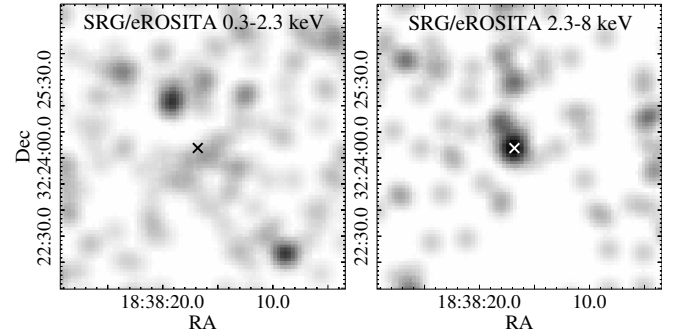


Figure 10. SRG/*eROSITA* images of the J1838 field in the 0.3–2.3 (left) and 2.3–8 (right) keV ranges. The data from the four scans are combined. The position of the J1838 likely optical counterpart is marked by the ‘X’ symbols.

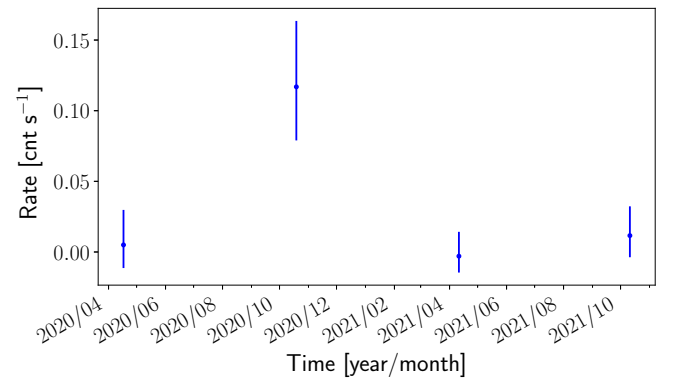


Figure 11. SRG *eROSITA* count rates of the J1838 putative counterpart in individual scans in the 2.3–8 keV band. The bright flare occurred in October 2020.

local density of variable sources can be different from a mean one, and it may depend on their maximum to minimum flux ratio.

Most RBs have light curves with two peaks per orbital cycle caused by tidal distortion of the companion, i.e. ellipsoidal variations. For BWs, irradiation from the pulsar wind is more significant than the tidal distortion effects which leads to the heating of the companion's side facing the pulsar and a single-peak light curve (e.g. [Draghis et al. 2019](#); [Swihart et al. 2022](#)). Usual light curve peak-to-peak amplitude is $\lesssim 1$ mag for RBs and 2–4 mag for BWs.

We have revealed that the optical and X-ray counterpart of J1838 proposed by [Kerby et al. \(2021\)](#) is a highly variable source demonstrating typical properties of spider systems. The presumed optical counterpart demonstrates brightness changes with a period of ≈ 4 h, resembling an orbital period of the expected spider system. It shows a single-peaked sine-like variability with a total amplitude of the brightness variation of about 3 mag (from ≈ 20 to ≈ 23 mag in the *R* band). At the same time, we found indications of its strong short-term flaring activity. The shape and amplitudes of the light curves are more typical for BWs. However, the RB interpretation of J1838 cannot be excluded since there is an example of a RB pulsar, J2339–0533, with an orbital period of 4.6 h, which also demonstrates single-peak light curves with a large difference between maxima and minima (e.g. $\Delta g \approx 6$ mag, [Kandel et al. 2020](#)). It was assumed to belong to the BW subclass until the pulsar discovery and measurements of the binary parameters ([Ray et al. 2020](#)).

From our light curve modelling of J1838, the derived Roche lobe filling factor is $f \approx 0.6$. It excludes any significant optical brightness variations related with the distorted shape of the companion. Nevertheless, it is also less than what is usually found for most spider systems, although there are objects with low values, e.g., PSR J0023+0923 with $f = 0.5 \pm 0.1$ ([Mata Sánchez et al. 2023](#)).

Our modelling also showed that J1838 demonstrates a significant difference between the night-side ($T_n \sim 2300$ K, corresponding to a M5–L4 type star) and day-side temperatures ($T_d \sim 11000$ K). RBs typically have $T_n = 4000$ – 6000 K (e.g. [Turchetta et al. 2023](#)) whereas BWs night sides are cooler, with $T_n = 1000$ – 3000 K (e.g. [Mata Sánchez et al. 2023](#)). In addition, RBs with their larger orbital periods usually have lower irradiation temperatures⁴ T_{irr} (several hundreds K) in comparison with BWs ($\gtrsim 3000$ K). A large T_{irr} of ≈ 6300 K was found for the above mentioned RB J2339–0533 with extreme heating ([Kandel et al. 2020](#)). However, this is still lower than what we obtained for J1838 ($T_{\text{irr}} \approx T_d^{\text{max}} = 10600$ K). The companion of the RB PSR J1816+4510 has an unusually high temperature of 16000 K ([Kaplan et al. 2013](#)) but its variability over the orbit is low ($\Delta G \sim 0.1$ mag; [Koljonen & Linares 2023](#)). There are several BW systems with T_{irr} of about 9000–10000 K, PSRs J1810+1744, J1555–2908 and J1641+8049 ([Romani et al. 2021](#); [Kennedy et al. 2022](#); [Mata Sánchez et al. 2023](#)), as well as the BW candidate ZTF J1406+1222 ([Burdge et al. 2022](#)). Overall, the temperature distribution of the J1838 companion is more typical for the BW family, although it is necessary to obtain higher resolution light curves to confirm this.

Rapid flaring in the optical revealed for J1838 is observed for some RB and BW systems: BW PSR J1311–3430 ([Romani 2012](#)), BW candidates 4FGL J0935.3+0901 ([Halpern 2022](#)) and 4FGL J1408.6–2917 ([Swihart et al. 2022](#)), RB PSR J1048+2339, RB candidates XMMU J083850.38–282756.8 and 1FGL J0523.5–2529 ([Cho, Halpern & Bogdanov 2018](#); [Halpern, Perez & Bogdanov 2022](#)).

⁴ The day-side temperature is related to the night-side and irradiation temperatures as $T_d^4 = T_n^4 + T_{\text{irr}}^4$.

The brightest ($\Delta \text{mag} \approx 1$) optical flare of J1838 was detected on 2022 July 24 (Fig. 6). The origin of such flares is not clear. They can be attributed to the variable emission from the intro-binary shocks between the pulsar and the companion created by the interaction of the pulsar wind and the wind ejected from the companion. Otherwise, they can be caused by an intrinsic companion magnetic activity as observed for low-mass stars (e.g. [Schmidt et al. 2019](#)).

The mass distribution of spider pulsars is bimodal with a gap in the range 0.07–0.1 M_\odot between BWs and RBs ([Swihart et al. 2022](#)). Thus, J1838 with $M_c = 0.10(5) M_\odot$ can belong to any of these subclasses. Better constraints on M_c are necessary to understand its spider type.

The distance obtained from the light curve modelling is about 3.1 kpc which is close to the upper bound of the distance range provided by *Gaia* (Table 1). The transverse velocity corresponding to this distance is about 200 km s⁻¹ which is at the upper bound of the velocity distribution for binary pulsar systems ([Hobbs et al. 2005](#)).

In X-rays, J1838 was firmly detected during two strong flares. Thus, we can estimate only an upper limit on its luminosity in quiescence, $L_X \lesssim 3.5 \times 10^{31} (D/3.1 \text{ kpc})^2 \text{ erg s}^{-1}$ and $\lesssim 10^{32} (D/3.1 \text{ kpc})^2 \text{ erg s}^{-1}$ for the PL model with the photon index appropriate for BWs and RBs, respectively. Studying X-ray properties of spider pulsars, [Swihart et al. \(2022\)](#) found that RBs are brighter than BWs with the average luminosities $L_X^{\text{rb}} = 2.3 \times 10^{32} \text{ erg s}^{-1}$ and $L_X^{\text{bw}} = 1.4 \times 10^{31} \text{ erg s}^{-1}$. The scatters of luminosities are rather wide and J1838 upper limits can be consistent with both subclasses.

Strong X-ray flares were observed for PSR J1311–3430, PSR J1048+2339, XMMU J083850.38–282756.8 and 1FGL J0523.5–2529 systems mentioned above. The brightest flares were detected for 1FGL J0523.5–2529 with the peak luminosities of $\sim 10^{34} \text{ erg s}^{-1}$, which is a factor of ~ 100 stronger than its minimum luminosity ([Halpern et al. 2022](#)). The X-ray flares of J1838 with the luminosity $L_X \sim 10^{34} (D/3.1 \text{ kpc})^2 \text{ erg s}^{-1}$ are at least two orders of magnitude (by a factor of 100–200) brighter than its quiescent emission. Its flare luminosity can be as large as for 1FGL J0523.5–2529, if the distance to the source is indeed 3.1 kpc. Thus, its flares can be the most luminous among the observed in RB/BW systems without accretion disks. The spectra of both flares are hard. It is interesting that the flare detected with *eROSITA* likely demonstrates a negative photon index. This possibly can be explained by an unresolved time lag between the hard and soft photon emission with a brighter outburst in the hard band.

Any alternative interpretation of the data, such as a cataclysmic variable (CV), a tight binary stellar system or a rotating magnetic star, appears to be very unlikely mainly due to the high modulation of the measured light curves. The former two demonstrate much flatter orbital light curves, sometimes with sharp dips due to binary companion eclipses (e.g., [Warner 1995](#); [Zasche et al. 2017](#), and references therein). For instance, light curves of intermediate polars (IPs), a subclass of CVs, typically show about 0.5 mag amplitude periodic variability. Sharp dips of 1–2 mag were observed in a few eclipsing IPs (e.g.: V597 Pup, [Warner & Woudt \(2009\)](#); IPHAS J062746.41+014811.3, [Aungwerjwit et al. \(2012\)](#); CXOGBS J174954.5–294335, [Johnson et al. \(2017\)](#)). Brightness variations of magnetic stars are typically less than a magnitude while rotational periods are greater than a day (e.g., [Bernhard et al. 2021](#)). Therefore, the spider pulsar interpretation currently remains the most plausible. This is also strongly supported by the detection of γ -rays which are not observed in the alternative cases. The fact that the estimated γ -ray luminosity of J1838 (Table 1) is within the range of luminosities ($4 \times 10^{32} - 4 \times 10^{34} \text{ erg s}^{-1}$) of the spider pulsar

family (Strader et al. 2019; Swihart et al. 2022) is in line with this interpretation.

Optical spectroscopy is needed to obtain the radial velocity curve of the J1838 companion candidate and confirm its nature. Accounting for its brightness, this is feasible with 8–10 meter class telescopes. RBs spectra are dominated by hydrogen lines while BWs spectra may show helium features indicating hydrogen-deficient atmospheres (Swihart et al. 2022 and references therein). Measurements of the companion’s radial velocity would provide constraints on the mass of the putative pulsar. High time-resolution multi-band light curves, especially in the minimum phase, would allow one to constrain the fundamental parameters of the binary system with a higher precision. To better understand the mechanism of flares simultaneous multicolour photometry would be preferable. Deeper X-ray observations are necessary to detect the object in quiescence. Last but not least, J1838 is of a particular interest for targeted searches of millisecond pulsations in the radio and/or γ -ray domains.

ACKNOWLEDGEMENTS

Based upon observations carried out at the Observatorio Astronómico Nacional on the Sierra San Pedro Mártir (OAN-SPM), Baja California, México. We thank the daytime and night support staff at the OAN-SPM for facilitating and helping obtain our observations. This work has made use of data from the European Space Agency (ESA) mission *Gaia* (<https://www.cosmos.esa.int/gaia>), processed by the *Gaia* Data Processing and Analysis Consortium (DPAC, <https://www.cosmos.esa.int/web/gaia/dpac/consortium>). Funding for the DPAC has been provided by national institutions, in particular the institutions participating in the *Gaia* Multilateral Agreement. Based on observations obtained with the Samuel Oschin Telescope 48-inch and the 60-inch Telescope at the Palomar Observatory as part of the Zwicky Transient Facility project. ZTF is supported by the National Science Foundation under Grants No. AST-1440341 and AST-2034437 and a collaboration including current partners Caltech, IPAC, the Weizmann Institute for Science, the Oskar Klein Center at Stockholm University, the University of Maryland, Deutsches Elektronen-Synchrotron and Humboldt University, the TANGO Consortium of Taiwan, the University of Wisconsin at Milwaukee, Trinity College Dublin, Lawrence Livermore National Laboratories, IN2P3, University of Warwick, Ruhr University Bochum, Northwestern University and former partners the University of Washington, Los Alamos National Laboratories, and Lawrence Berkeley National Laboratories. Operations are conducted by COO, IPAC, and UW. This work used data obtained with eROSITA telescope onboard SRG observatory. The SRG observatory was built by Roskosmos in the interests of the Russian Academy of Sciences represented by its Space Research Institute (IKI) in the framework of the Russian Federal Space Program, with the participation of the Deutsches Zentrum für Luft- und Raumfahrt (DLR). The SRG/eROSITA X-ray telescope was built by a consortium of German Institutes led by MPE, and supported by DLR. The SRG spacecraft was designed, built, launched and is operated by the Lavochkin Association and its subcontractors. The science data are downlinked via the Deep Space Network Antennae in Bear Lakes, Ussurijsk, and Baykonur, funded by Roskosmos. The eROSITA data used in this work were processed using the eSASS software system developed by the German eROSITA consortium and proprietary data reduction and analysis software developed by the Russian eROSITA Consortium.

We are grateful to the anonymous referee for useful comments allowing us to improve the paper. The work of DAZ and AVK was

supported by the Russian Science Foundation, grant number 22-22-00921, <https://rscf.ru/project/22-22-00921/>. DAZ thanks Pirinem School of Theoretical Physics for hospitality. SVZ acknowledges PAPIIT grant IN119323.

DATA AVAILABILITY

The *Swift* data are available through the archive https://www.swift.ac.uk/swift_portal/, ZTF data – <https://irsa.ipac.caltech.edu/Missions/ztf.html>, eROSITA and OAN-SPM data – on request.

REFERENCES

- Abdollahi S., et al., 2022, *ApJS*, 260, 53
 Ablimit I., 2019, *ApJ*, 881, 72
 Archibald A. M., et al., 2009, *Science*, 324, 1411
 Arnaud K. A., 1996, in Jacoby G. H., Barnes J., eds, *Astronomical Society of the Pacific Conference Series Vol. 101, Astronomical Data Analysis Software and Systems V*. p. 17
 Au K.-Y., et al., 2023, *ApJ*, 943, 103
 Aungwerojwit A., Gänsicke B. T., Wheatley P. J., Pyrzas S., Staels B., Krajci T., Rodríguez-Gil P., 2012, *ApJ*, 758, 79
 Bassa C. G., et al., 2014, *MNRAS*, 441, 1825
 Benvenuto O. G., De Vito M. A., Horvath J. E., 2014, *ApJ*, 786, L7
 Bernhard K., Hümmerich S., Paunzen E., Supíková J., 2021, *MNRAS*, 506, 4561
 Burdge K. B., et al., 2022, *Nature*, 605, 41
 Chen H.-L., Chen X., Tauris T. M., Han Z., 2013, *ApJ*, 775, 27
 Cho P. B., Halpern J. P., Bogdanov S., 2018, *ApJ*, 866, 71
 Draghis P., Romani R. W., Filippenko A. V., Brink T. G., Zheng W., Halpern J. P., Camilo F., 2019, *ApJ*, 883, 108
 Evans P. A., et al., 2009, *MNRAS*, 397, 1177
 Flewelling H. A., et al., 2020, *ApJS*, 251, 7
 Foight D. R., Güver T., Özel F., Slane P. O., 2016, *ApJ*, 826, 66
 Gaia Collaboration et al., 2016, *A&A*, 595, A1
 Gaia Collaboration et al., 2021, *A&A*, 649, A1
 Green G. M., Schlafly E., Zucker C., Speagle J. S., Finkbeiner D., 2019, *ApJ*, 887, 93
 Guo Y., Wang B., Han Z., 2022, *MNRAS*, 515, 2725
 Halpern J. P., 2022, *ApJ*, 932, L8
 Halpern J. P., Perez K. I., Bogdanov S., 2022, *ApJ*, 935, 151
 Hobbs G., Lorimer D. R., Lyne A. G., Kramer M., 2005, *MNRAS*, 360, 974
 Johnson C. B., et al., 2017, *MNRAS*, 466, 129
 Kandel D., Romani R. W., Filippenko A. V., Brink T. G., Zheng W., 2020, *ApJ*, 903, 39
 Kaplan D. L., Bhalerao V. B., van Kerkwijk M. H., Koester D., Kulkarni S. R., Stovall K., 2013, *ApJ*, 765, 158
 Karpova A. V., Zyuzin D. A., Shibanov Y. A., Gilfanov M. R., 2023, *MNRAS*, 524, 3020
 Kennedy M. R., et al., 2022, *MNRAS*, 512, 3001
 Kerby S., et al., 2021, *ApJ*, 923, 75
 Koljonen K. I. I., Linares M., 2023, arXiv e-prints, p. [arXiv:2308.07377](https://arxiv.org/abs/2308.07377)
 Lampton M., Margon B., Bowyer S., 1976, *ApJ*, 208, 177
 Landolt A. U., 1992, *AJ*, 104, 340
 Linares M., Shahbaz T., Casares J., 2018, *ApJ*, 859, 54
 Lindgren L., et al., 2021, *A&A*, 649, A2
 Lomb N. R., 1976, *Ap&SS*, 39, 447
 Masci F. J., et al., 2019, *PASP*, 131, 018003
 Mata Sánchez D., et al., 2023, *MNRAS*, 520, 2217
 Medvedev P. S., Gilfanov M. R., Sazonov S. Y., Sunyaev R. A., Khorunzhev G. A., 2022, *Astronomy Letters*, 48, 735
 Miller J. M., et al., 2020, *ApJ*, 904, 49
 Papitto A., et al., 2013, *Nature*, 501, 517
 Predehl P., et al., 2021, *A&A*, 647, A1

- Ray P. S., et al., 2020, *Research Notes of the American Astronomical Society*, **4**, 37
- Roberts M. S. E., 2013, in van Leeuwen J., ed., Vol. 291, *Neutron Stars and Pulsars: Challenges and Opportunities after 80 years*. pp 127–132 ([arXiv:1210.6903](https://arxiv.org/abs/1210.6903)), doi:10.1017/S174392131202337X
- Romani R. W., 2012, *ApJ*, **754**, L25
- Romani R. W., Kandel D., Filippenko A. V., Brink T. G., Zheng W., 2021, *ApJ*, **908**, L46
- Romani R. W., Kandel D., Filippenko A. V., Brink T. G., Zheng W., 2022, *ApJ*, **934**, L17
- Roy J., et al., 2015, *ApJ*, **800**, L12
- Salvetti D., et al., 2017, *MNRAS*, **470**, 466
- Scargle J. D., 1982, *ApJ*, **263**, 835
- Schmidt S. J., et al., 2019, *ApJ*, **876**, 115
- Smith D. A., et al., 2023, arXiv e-prints, p. [arXiv:2307.11132](https://arxiv.org/abs/2307.11132)
- Strader J., et al., 2019, *ApJ*, **872**, 42
- Sunyaev R., et al., 2021, *A&A*, **656**, A132
- Swihart S. J., et al., 2020, *ApJ*, **892**, 21
- Swihart S. J., Strader J., Aydi E., Chomiuk L., Dage K. C., Shishkovsky L., 2021, *ApJ*, **909**, 185
- Swihart S. J., Strader J., Chomiuk L., Aydi E., Sokolovsky K. V., Ray P. S., Kerr M., 2022, *ApJ*, **941**, 199
- Turchetta M., Linares M., Koljonen K., Sen B., 2023, arXiv e-prints, p. [arXiv:2307.06330](https://arxiv.org/abs/2307.06330)
- Warner B., 1995, *Cataclysmic variable stars*. Vol. 28, Cambridge University Press
- Warner B., Woudt P. A., 2009, *MNRAS*, **397**, 979
- Wilms J., Allen A., McCray R., 2000, *ApJ*, **542**, 914
- Yap Y. X. J., Kong A., Li K. L., 2023, arXiv e-prints, p. [arXiv:2307.13482](https://arxiv.org/abs/2307.13482)
- Zasche P., Wolf M., Vraštil J., 2017, *MNRAS*, **469**, 2952
- Zharikov S., Tovmassian G., Aviles A., Michel R., Gonzalez-Buitrago D., García-Díaz M. T., 2013, *A&A*, **549**, A77
- Zharikov S., Kirichenko A., Zyuzin D., Shibanov Y., Deneva J. S., 2019, *MNRAS*, **489**, 5547

This paper has been typeset from a $\text{\TeX}/\text{\LaTeX}$ file prepared by the author.